Solvent Effects on Structure and Screening in Confined Electrolytes

Jie Yang,[1,2] Svyatoslav Kondrat,[1,3,*] Cheng Lian,[2,†] Honglai Liu,[2] Alexander Schlaich,[1,4,‡] and Christian Holm[1,§]
[1]Institute for Computational Physics, University of Stuttgart, 70569 Stuttgart, Germany
[2]School of Chemistry and Molecular Engineering, East China University of Science and Technology, Shanghai 200237, China
[3]Institute of Physical Chemistry, Polish Academy of Sciences, 01-224 Warsaw, Poland
[4]Stuttgart Center for Simulation Science (SC SimTech), University of Stuttgart, 70569 Stuttgart, Germany

(Received 28 February 2023; revised 4 July 2023; accepted 15 August 2023; published 11 September 2023)

Using classical density functional theory, we investigate the influence of solvent on the structure and ionic screening of electrolytes under slit confinement and in contact with a reservoir. We consider a symmetric electrolyte with implicit and explicit solvent models and find that spatially resolving solvent molecules is essential for the ion structure at confining walls, excess ion adsorption, and the pressure exerted on the walls. Despite this, we observe only moderate differences in the period of oscillations of the pressure with the slit width and virtually coinciding decay lengths as functions of the scaling variable $\sigma_{\text{ion}}/\lambda_D$, where σ_{ion} is the ion diameter and λ_D the Debye length. Moreover, in the electrostatic-dominated regime, this scaling behavior is practically independent of the relative permittivity and its dependence on the ion concentration. In contrast, the crossover to the hard-core-dominated regime depends sensitively on all three factors.

DOI: 10.1103/PhysRevLett.131.118201

Introduction.—Recent surface force balance (SFB) experiments [1–3], suggesting anomalously large screening lengths for concentrated electrolytes and room-temperature ionic liquids (ILs), have revived the interest in ionic screening in such systems. Despite the significant effort by various experimental [4–7], theoretical [8–13], and simulation [14–17] groups, the existence of anomalously long screening lengths remains a mystery [18]. Most of the recent theoretical [8–10] and simulation [14–16] works are consistent with classical theories developed in the mid-1990s [19,20] and show no signs of anomalously large screening lengths.

At low ion densities, the screening of electrolyte-mediated interactions is determined by the Debye length, which for monovalent ions is

$$\lambda_D = \sqrt{\frac{\epsilon_0 \epsilon_r k_B T}{e^2 \rho}} = (4\pi l_B \rho)^{-1/2}, \tag{1}$$

where $\rho = \rho_+ + \rho_-$ is the total ion concentration ($\rho_+ = \rho_-$ are the cation and anion concentrations), ϵ_0 is the vacuum and ϵ_r the relative permittivity, k_B is the Boltzmann constant and T temperature, e the proton charge, and $l_B = e^2/(4\pi\epsilon_0\epsilon_r k_B T)$ is the Bjerrum length. As the ion density ρ increases, the leading-order screening length deviates from the Debye length and, from a certain point on, increases with ρ. This point, known as the Kirkwood crossover, is determined by the emergence of a damped oscillatory behavior in the charge-charge correlation function [19,20]. At yet higher densities, there is a crossover from this charge-dominated screening to the screening determined by hard-core interactions [10,19,21].

Most theoretical and simulation studies so far have considered neat ionic liquids or treated the solvent as an effective dielectric medium [8,10,11,17,22]. However, in practical applications, ions are frequently mixed with a solvent that affects ionic correlations directly through screening of the bare Coulomb interactions and indirectly through excluded volumes. The role of excluded volume interactions has recently been analyzed by Coupette *et al.* [23]. These authors considered a hard sphere model for the solvent molecules but assumed that the relative dielectric permittivity is independent of the solvent and ion densities. Within these assumptions, they found multiple decay lengths coexisting in the asymptotic limit and at intermediate distances, determined by the ion and solvent molecular sizes. All-atom simulations with various solvents also resolve multiple decay lengths [15,16].

In this Letter, we use classical density functional theory (DFT) to study how a solvent affects the screening of electrolyte-mediated interactions between confining charged walls. We consider implicit and explicit solvent models and find that both models predict the same screening lengths when electrostatic interactions dominate the screening. Nevertheless, spatially resolving solvent molecules becomes essential for ionic structure and forces at short separations. We also find that the dielectric properties of the solvent play a crucial role in the crossover from the electrostatic-dominated to the hard core-dominated screening regime that occurs when the ion density increases.

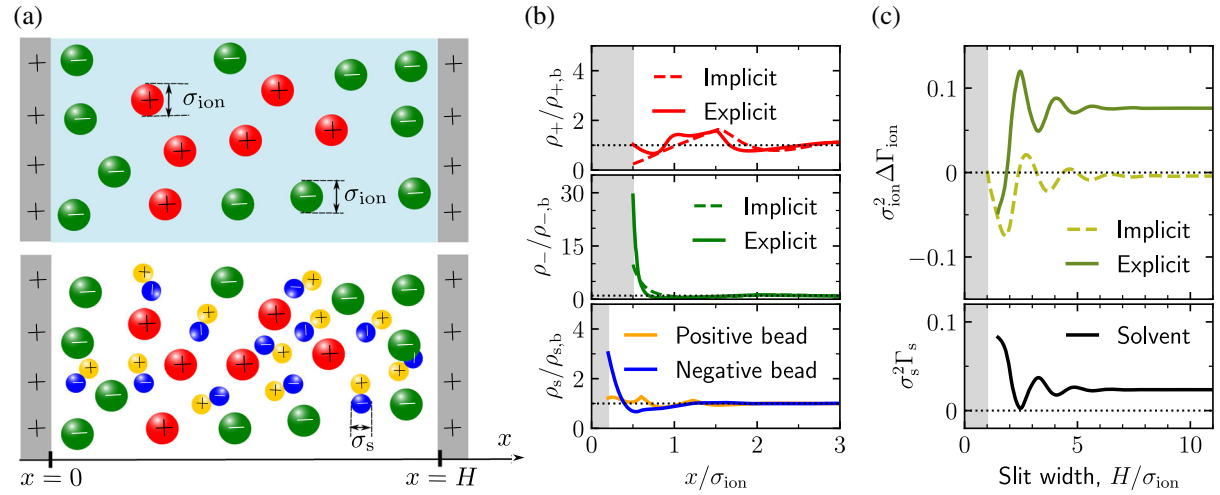

FIG. 1. Implicit and explicit solvent models and density profiles of confined electrolytes. (a) Schematics of two charged plates confining an electrolyte with implicit (top) and explicit (bottom) solvent models. Cations and anions have the same diameter $\sigma_{\rm ion}$ and the solvent consists of two touching oppositely charged beads of the same diameter $\sigma_{\rm s}$. x denotes the coordinate perpendicular to two plates separated by distance H. (b) Density profiles of cations (top), anions (middle), and solvent beads (bottom) for bulk ion density $\rho_{\rm b} = 4\,{\rm M}$ (salt concentration 2M) and $H/\sigma_{\rm ion} = 6$. The gray rectangles show the areas excluded to the center of ions (top and middle) and solvent beads (bottom). (c) Excess adsorption $\Delta\Gamma_{\rm ion} = \Gamma_{\rm ion} - 2Q/e$ [Eq. (3)] for the ions (top) and $\Gamma_{\rm s}$ for the solvent (bottom) as functions of the plate-plate separation H at $\rho_{\rm b} = 4\,{\rm M}$. Ion diameter $\sigma_{\rm ion} = 0.5$ nm, surface charge $Q = 0.5\ {\rm e/nm^2}$, and temperature $T = 293$ K. For the implicit solvent calculations, we have chosen $\epsilon_r = 9.8$, as estimated by a dielectric capacitor model for the explicit solvent (see the main text).

Models and methods.—We modeled ions as charged hard spheres of equal diameter $\sigma_{\rm ion} = 0.5$ nm. For the explicit solvent model, we considered dumbbell-like solvent molecules, as suggested by Henderson *et al.* [24], consisting of two oppositely charged beads $s\pm$ of charge $q_{s\pm} = \pm 0.1926$ and the same diameter $\sigma_{\rm s} = 0.2$ nm separated by distance 0.2 nm yielding a dipole moment of 1.85D [Fig. 1(a)]. Following their approach, we used a background dielectric permittivity $\varepsilon_{\rm b} = 4.1$ (corresponding to rescaling all charges by a factor ≈ 0.5) to enhance numerical convergence. The electrolyte was confined between two identical positively charged walls with the surface charge density $Q = 0.5\ {\rm e/nm^2}$ (see Sec. S1 in the Supplemental Material [25] for details).

Within DFT, the densities of species $i = \{+, -, s+, s-\}$ can be obtained by solving the nonlinear equations

$$\rho_i = \exp\left\{\beta\mu_i - \beta U_i - \frac{\delta\beta F_{\rm ex}[\{\rho_i\}]}{\delta\rho_i}\right\}, \tag{2}$$

where μ_i is the chemical potential, U_i is an external electrostatic potential acting on species i due to the confining walls, and $F_{\rm ex}$ is the density-dependent excess free energy functional. We considered $F_{\rm ex}$ consisting of three contributions: (1) hard-core interactions modeled with modified fundamental measure theory, which is known to describe these interactions remarkably well [26,27,38]; (2) electrostatic interactions modeled on the level of the mean spherical approximation (MSA) [39,40]; and (3) in the case of an explicit solvent, $F_{\rm ex}$ also contained a contribution due to the bonding potential between the two beads of a solvent molecule (see Sec. S2 in the Supplemental Material [25]). To relate the densities ρ_i in bulk to μ_i, we performed calculations for the bulk electrolyte at temperature $T = 293$ K and a given bulk ion density $\rho_{\rm b}$. With these μ_i at hand, we solved Eq. (2) numerically for an electrolyte (with explicit and implicit solvents) confined between two plates at separation H using the Picard iteration method [28].

For the explicit solvent, we estimated the dielectric permittivity using a dielectric capacitor model, which gave $\epsilon_r \approx 9.8$ (see Sec. S3 in the Supplemental Material [25]); this result is in reasonable agreement with molecular dynamics simulations of the same model [29]. To investigate how an explicit solvent affects the molecular structure and ionic screening, we used $\epsilon_r = 9.8$ in the corresponding implicit solvent calculations. However, we also considered other values of ϵ_r—and particularly its concentration dependence—to study how it affects ionic screening.

Implicit vs explicit solvent: Ion densities.—Exemplary ion and solvent density profiles are presented in Fig. 1(b), which show that spatially resolving solvent molecules considerably affects the arrangement of ions at the surface. Instead of decreasing when approaching the surface, as in the implicit solvent model, the coion (cation in our case) density shows a nonmonotonic behavior, exhibiting an additional small peak and an increase at the surface. This behavior is due to the presence of dipoles, which are oriented predominantly perpendicularly to the surface,

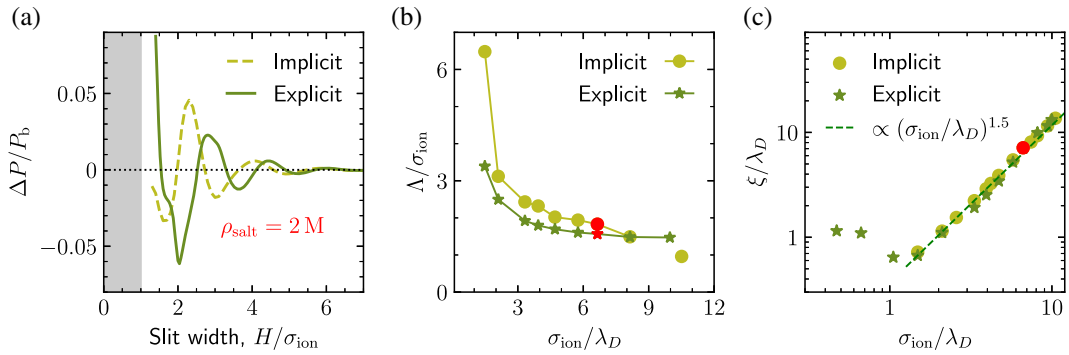

FIG. 2. Implicit vs explicit solvent models: Pressure and screening behavior. (a) Relative pressure difference $\Delta P/P_{\rm b}$ (where $\Delta P = P - P_{\rm b}$ and $P_{\rm b}$ is the bulk pressure) as a function of slit width H for the bulk ion density $\rho_{\rm b} = 4\,\mathrm{M}$ (salt concentration $\rho_{\rm salt} = 2\,\mathrm{M}$). The gray area shows separations $H < \sigma_{\rm ion}$, where $\sigma_{\rm ion}$ is the ion diameter. (b) Period of oscillations Λ and (c) decay length ξ as functions of the scaling variable $\sigma_{\rm ion}/\lambda_D$ obtained from fitting the numerical DFT results for the pressure by Eq. (4). The red symbols in panels (b) and (c) denote the salt concentration 2M used in panel (a). The parameters are the same as in Fig. 1.

partially screening the surface charge and attracting more coions to the surface [Fig. 1(b), bottom plot].

While both models predict a similar structure for the counterion (anion) density, its value at the surface is nearly three times higher for the explicit solvent model. Atomistic simulations of polar and apolar aqueous interfaces have reported oscillatory behavior of the anisotropic dielectric response tensor, which strongly modifies the ionic free energy profiles [30,41], in line with an effective reduction of the dielectric constant [31]. Note that such a decrease of the dielectric constant close to the interface and the corresponding increase of the counterion density can also be accounted for on a mean-field level by taking into account excluded volume and solvent polarization effects [42] or via a special simulation strategy [43,44]. Such effects, however, are not captured by our implicit solvent model, which rationalizes the qualitatively different interfacial ion density profiles in Fig. 1(b).

The difference in the counterion densities within the two models manifests itself in the excess ion adsorption,

$$\Gamma_{\rm ion} = \int_{\sigma_{\rm ion}/2}^{H-\sigma_{\rm ion}/2} [\rho(x) - \rho_{\rm b}]dx, \tag{3}$$

which we defined such that it yields zero when the ion density equals the bulk ion density. Since the slit walls are charged, it is convenient to subtract from $\Gamma_{\rm ion}$ the contribution of the counterions. In Fig. 1(c), therefore, we show $\Delta\Gamma_{\rm ion} = \Gamma_{\rm ion} - 2Q/e$. For the implicit solvent model, the excess adsorption practically vanishes for large slits, corresponding to a semi-infinite system; note that it is not exactly zero likely due to the differences in nonelectrostatic (mainly steric in our case) interactions in the bulk and at the wall. In accord with the density profiles, $\Delta\Gamma_{\rm ion}$ is substantially larger than zero for the explicit solvent model. Within both models, however, $\Delta\Gamma_{\rm ion}$ shows a damped oscillatory behavior related to ion layering and "quantized" expulsion of ionic layers with decreasing H [45]. Correspondingly, the amplitude of oscillations increases when H decreases. For the explicit solvent model, the excess solvent adsorption, $\Gamma_{\rm s} = \int_{\sigma_{\rm s}/2}^{H-\sigma_{\rm s}/2} [\rho_{\rm s}(x) - \rho_{\rm s,b}]dx$, shows a similar behavior [Fig. 1(c)].

Implicit vs explicit solvent: Electrolyte-mediated forces.—From the density profiles, we computed the force per surface area (i.e., the pressure) exerted on the confining walls within the two models (see Sec. S2 in the Supplemental Material [25]). Figure 2(a) shows that spatially resolving the solvent molecules is essential for the pressure behavior at short distances. For the implicit model, the pressure shows peaks at separations slightly larger than $2\sigma_{\rm ion}$, $4\sigma_{\rm ion}$, etc. For the explicit solvent model, these peaks are shifted towards larger separations because the presence of solvent molecules enlarges the sizes of molecular layers. The peaks are also more extended, showing small shoulders, which is due to an additional expulsion of solvent molecules as the slit width decreases.

To extract screening lengths, we fitted the DFT data for the pressure at large plate-plate separation to (see Fig. S2 in the Supplemental Material [25] for examples)

$$P(H) \approx P_{\rm b} + Ae^{-H/\xi}\cos(2\pi H/\Lambda + \phi), \tag{4}$$

where A is the amplitude, Λ and ϕ are the period of oscillations and the phase shift, respectively, and ξ is the decay length, all treated as fitting parameters. In Figs. 2(b) and 2(c), we plot the results for Λ and ξ. The oscillation periods show similar qualitative but different quantitative behaviors in the two models. At low densities, the implicit solvent model predicts Λ nearly twice as large its value obtained with the explicit solvent model. This behavior suggests that spatially resolving solvent molecules shift the Kirkwood point towards lower densities. In both models, Λ decreases with increasing the ion concentration, albeit saturating at different values. While in the implicit solvent model, Λ approaches the ion diameter, in the explicit solvent, the oscillation period is larger due to the presence

of solvent molecules in the ionic structure [Figs. 1(b) and 1(c)], which is reflected in the behavior of pressure.

Figure 2(c) shows the screening lengths ξ plotted using the scaling variables ξ/λ_D and $\sigma_{\text{ion}}/\lambda_D$. The screening lengths within both approaches practically coincide. While it may seem surprising at first sight, this agreement between the two models is because the electrostatic interactions, which determine the screening in the considered concentration range, are the same in both models. For concentrations above the Kirkwood point ($\sigma_{\text{ion}}/\lambda_D \approx 1.25$), the screening lengths increase with the IL concentration in both cases. The fitting yields a scaling law

$$\xi/\lambda_D \sim (\sigma_{\text{ion}}/\lambda_D)^n, \tag{5}$$

where the scaling exponent $n \approx 1.5$ is consistent with previous MSA results [9].

Effect of relative dielectric permittivity.—Since explicit and implicit solvent models predict virtually the same correlation lengths ξ [Fig. 2(c)], we further consider only the implicit solvent model, characterized by a relative dielectric permittivity ϵ_r and study how ϵ_r influences the scaling behavior of ξ. Figure 3(a) shows the correlation lengths for a few values of ϵ_r, from $\epsilon_r = 9.8$, as in Figs. 1 and 2, to $\epsilon_r = 78$, corresponding to water at room temperature ($T = 293$ K). Above the Kirkwood crossover at $\sigma_{\text{ion}}/\lambda_D \approx 1.5$, the screening lengths increase with concentration, as expected, showing the $n = 1.5$ scaling exponent. However, in the systems with higher permittivity ($\epsilon_r \gtrsim 40$), the correlation lengths start deviating from the $n = 1.5$ scaling behavior. This deviation occurs at a lower concentration for a higher permittivity and is related to a crossover from the electrostatic-dominated to hard-core–dominated screening [10]. To illustrate this crossover, we determined the decay lengths ξ_ρ and ξ_c of the total density ρ and charge density $c = e(\rho_+ - \rho_-)$ at a single wall (we used confined systems but of a large slit width $H/\sigma_{\text{ion}} \geq 16$, see Sec. S4 in the Supplemental Material [25]). Orange lines and symbols in Fig. 3(a) show these decay lengths for $\epsilon_r = 78$, demonstrating that ξ_c coincides with the screening length ξ (determined from the H dependence of the pressure) for $\sigma_{\text{ion}}/\lambda_D \lesssim 3$, while $\xi \approx \xi_\rho$ above this threshold value. Thus, at $\sigma_{\text{ion}}/\lambda_D \approx 3$, there is a crossover between the charge-dominated and density-dominated regimes.

Ion concentration-dependent relative permittivity.—So far, we have assumed a constant relative permittivity ϵ_r independent of the ion concentration. However, it is known that the presence of ions changes ϵ_r [46–50]. To investigate how the concentration dependence of ϵ_r influences ionic screening, we considered aqueous electrolytes and performed DFT calculations for $\epsilon_r = 78$, corresponding to water at room temperature (with no ions), and for $\epsilon_r(\rho) = -0.031\rho^3 + 1.322\rho^2 - 13.44\rho + 80.84$, which describes the measured dielectric permittivity of water as a function of the concentration of NaCl at $T = 293$ K (see Refs. [50];

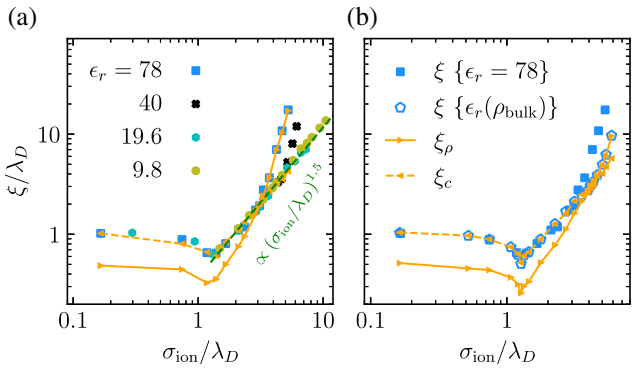

FIG. 3. Effect of the relative permittivity of the solvent. (a) Screening lengths ξ expressed in terms of the Debye length λ_D as functions of $\sigma_{\text{ion}}/\lambda_D$ for several values of the dielectric constant ϵ_r, assumed ion concentration independent. The green dashed line indicates the scaling power law $\xi/\lambda_D \propto (\sigma_{\text{ion}}/\lambda_D)^{1.5}$. (b) Screening lengths in aqueous electrolytes for a constant dielectric permittivity $\epsilon_r = 78$ [as in panel (a)] and when ϵ_r depends on the ion concentration (see the main text for the equation). The orange lines and symbols show the screening lengths obtained for large slit width ($H/\sigma_{\text{ion}} \geq 16$) from the decay of the total ion density (ξ_ρ) and charge density (ξ_c) with the distance from the wall for $\epsilon_r = 78$ [panel (a)] and $\epsilon_r(\rho_{\text{b}})$ [panel (b)]. The parameters are the same as in Fig. 1.

$\epsilon_r(\rho = 0) = 80.84$ slightly differs from the value $\epsilon_r = 78$ used in the constant ϵ_r calculations, but this small difference barely affects the results). Note that we neglected the spatial variation of ϵ_r due to the spatially varying ion density, assuming the same ϵ_r throughout the cell evaluated at the bulk ion density ρ_{b}.

Figure 3(b) (blue symbols) shows that ξ/λ_D deviates from the $n = 1.5$ scaling behavior at a higher ion concentration (larger $\sigma_{\text{ion}}/\lambda_D$) in the case of the concentration-dependent permittivity. The orange lines and symbols in Fig. 3(b) show the decay lengths ξ_ρ and ξ_c, demonstrating that the deviation from the $n = 1.5$ scaling is again due to a crossover from the charge-dominated to density-dominated regime. However, compared with the concentration-independent ϵ_r, this crossover is shifted towards higher ion densities because the presence of ions reduces ϵ_r, enhancing the electrostatic interactions and extending the electrostatics-dominated regime.

Conclusions.—We have demonstrated that modeling a solvent explicitly is essential in determining the molecular structure of confined electrolytes, the ion adsorption, and the electrolyte-mediated forces between confining walls (Fig. 1). However, explicit and implicit solvent models predict the same screening lengths at ion concentrations at which the electrostatic interactions dominate the forces (Fig. 2). In this regime, the screening lengths are independent of the dielectric permittivity and its variation with the ion concentration and follow the scaling law given by Eq. (5) with $n = 1.5$. This scaling exponent agrees with previous MSA results [9], but differs from the scaling exponents

reported in other works, viz., $n = 1$ (Refs. [9,12,15]), $n = 2$ (Refs. [8,12,15]), $n \approx 1.3$ (Ref. [14]), $n = 5$ (Ref. [12]), and $n = 3$ exponent [12,51]; which exponent is correct and whether there is a single well-defined exponent remains to be seen. We note that the screening lengths obtained in our work are significantly smaller than reported by SFB experiments of Refs. [1–3] but consistent with other (particularly AFM) experiments, which do not show underscreening [6,7].

At higher ion concentrations, we observed a crossover from the electrostatic-dominated screening to the screening dominated by hard-core interactions (Fig. 3). Our calculations revealed that the crossover location depends sensitively on the solvent model, the relative dielectric permittivity of the solvent, and its concentration dependence. Unlike in the electrostatic-dominated regime, we have not found any scaling law akin to Eq. (5) in the hard-core dominated regime.

A. S. and C. H. were funded by the Deutsche Forschungsgemeinschaft (DFG, German Research Foundation) under Germany's Excellence Strategy—EXC 2075–390740016 and SFB 1333/2–358283783. S. K. acknowledges the financial support by NCN Grants No. 2020/39/I/ST3/02199 and No. 2021/40/Q/ST4/00160. J. Y., C. L., and H. L. acknowledge Grant No. NSFC (22078088).

*svyatoslav.kondrat@gmail.com; skondrat@ichf.edu.pl
†liancheng@ecust.edu.cn
‡schlaich@icp.uni-stuttgart.de
§holm@icp.uni-stuttgart.de

[1] M. A. Gebbie, M. Valtiner, X. Banquy, E. T. Fox, W. A. Henderson, and J. N. Israelachvili, Ionic liquids behave as dilute electrolyte solutions, Proc. Natl. Acad. Sci. U.S.A. **110**, 9674 (2013).
[2] M. A. Gebbie, H. A. Dobbs, M. Valtiner, and J. N. Israelachvili, Long-range electrostatic screening in ionic liquids, Proc. Natl. Acad. Sci. U.S.A. **112**, 7432 (2015).
[3] A. M. Smith, A. A. Lee, and S. Perkin, The electrostatic screening length in concentrated electrolytes increases with concentration, J. Phys. Chem. Lett. **7**, 2157 (2016).
[4] P. Gaddam and W. Ducker, Electrostatic screening length in concentrated salt solutions, Langmuir **35**, 5719 (2019).
[5] H. Yuan, W. Deng, X. Zhu, G. Liu, and V. S. J. Craig, Colloidal systems in concentrated electrolyte solutions exhibit re-entrant long-range electrostatic interactions due to underscreening, Langmuir **38**, 6164 (2022).
[6] T. Baimpos, B. R. Shrestha, S. Raman, and M. Valtiner, Effect of interfacial ion structuring on range and magnitude of electric double layer, hydration, and adhesive interactions between mica surfaces in 0.05–3 m Li^+ and Cs^+ electrolyte solutions, Langmuir **30**, 4322 (2014).
[7] S. Kumar, P. Cats, M. B. Alotaibi, S. C. Ayirala, A. A. Yousef, R. van Roij, I. Siretanu, and F. Mugele, Absence of anomalous underscreening in highly concentrated aqueous electrolytes confined between smooth silica surfaces, J. Colloid Interface Sci. **622**, 819 (2022).
[8] R. M. Adar, S. A. Safran, H. Diamant, and D. Andelman, Screening length for finite-size ions in concentrated electrolytes, Phys. Rev. E **100**, 042615 (2019).
[9] B. Rotenberg, O. Bernard, and J.-P. Hansen, Underscreening in ionic liquids: A first principles analysis, J. Phys. Condens. Matter **30**, 054005 (2018).
[10] P. Cats, R. Evans, A. Härtel, and R. van Roij, Primitive model electrolytes in the near and far field: Decay lengths from DFT and simulations, J. Chem. Phys. **154**, 124504 (2021).
[11] A. Ciach and O. Patsahan, Correct scaling of the correlation length from a theory for concentrated electrolytes, J. Phys. Condens. Matter **33**, 37LT01 (2021).
[12] A. Ciach and O. Patsahan, Structure of ionic liquids and concentrated electrolytes from a mesoscopic theory, J. Mol. Liq. **377**, 121453 (2023).
[13] O. Patsahan and A. Ciach, Mesoscopic inhomogeneities in concentrated electrolytes, ACS Omega **7**, 6655 (2022).
[14] S. W. Coles, C. Park, R. Nikam, M. Kanduč, J. Dzubiella, and B. Rotenberg, Correlation length in concentrated electrolytes: Insights from all-atom molecular dynamics simulations, J. Phys. Chem. B **124**, 1778 (2020).
[15] J. Zeman, S. Kondrat, and C. Holm, Bulk ionic screening lengths from extremely large-scale molecular dynamics simulations, Chem. Commun. **56**, 15635 (2020).
[16] J. Zeman, S. Kondrat, and C. Holm, Ionic screening in bulk and under confinement, J. Chem. Phys. **155**, 204501 (2021).
[17] A. Härtel, M. Bültmann, and F. Coupette, Anomalous Underscreening in the Restricted Primitive Model, Phys. Rev. Lett. **130**, 108202 (2023).
[18] C. Holm and S. Kondrat, The mystery of anomalously long-ranged screening in concentrated ionic systems, J. Club Condens. Matter Phys. 10.36471/jccm_november_2022_02 (2022).
[19] P. Attard, Asymptotic analysis of primitive model electrolytes and the electrical double layer, Phys. Rev. E **48**, 3604 (1993).
[20] R. Evans, R. J. F. L. de Carvalho, J. R. Henderson, and D. C. Hoyle, Asymptotic decay of correlations in liquids and their mixtures, J. Chem. Phys. **100**, 591 (1994).
[21] R. L. de Carvalho and R. Evans, The decay of correlations in ionic fluids, Mol. Phys. **83**, 619 (1994).
[22] K. Ma, C. Lian, C. E. Woodward, and B. Qin, Classical density functional theory reveals coexisting short-range structural decay and long-range force decay in ionic liquids, Chem. Phys. Lett. **739**, 137001 (2020).
[23] F. Coupette, A. A. Lee, and A. Härtel, Screening Lengths in Ionic Fluids, Phys. Rev. Lett. **121**, 075501 (2018).
[24] D. Henderson, D.-e. Jiang, Z. Jin, and J. Wu, Application of density functional theory to study the double layer of an electrolyte with an explicit dimer model for the solvent, J. Phys. Chem. B **116**, 11356 (2012).
[25] See Supplemental Material at http://link.aps.org/supplemental/10.1103/PhysRevLett.131.118201 for details of the solvent model and DFT calculations, the determination of the effective dielectric permittivity and the decay lengths of density profiles, and Supplementary plots, which includes Refs. [24,26–37].

[26] Y.-X. Yu and J. Wu, Structures of hard-sphere fluids from a modified fundamental-measure theory, J. Chem. Phys. **117**, 10156 (2002).
[27] R. Roth, R. Evans, A. Lang, and G. Kahl, Fundamental measure theory for hard-sphere mixtures revisited: The white bear version, J. Phys. Condens. Matter **14**, 12063 (2002).
[28] J. Mairhofer and J. Gross, Numerical aspects of classical density functional theory for one-dimensional vapor-liquid interfaces, Fluid Phase Equilib. **444**, 1 (2017).
[29] H. Jäger, A. Schlaich, J. Yang, C. Lian, S. Kondrat, and C. Holm, A screening of results on the decay length in concentrated electrolytes, Faraday Discuss. (2023).
[30] P. Loche, C. Ayaz, A. Wolde-Kidan, A. Schlaich, and R. R. Netz, Universal and nonuniversal aspects of electrostatics in aqueous nanoconfinement, J. Phys. Chem. B **124**, 4365 (2020).
[31] A. Schlaich, E. W. Knapp, and R. R. Netz, Water Dielectric Effects in Planar Confinement, Phys. Rev. Lett. **117**, 048001 (2016).
[32] C. E. Woodward, A density functional theory for polymers: Application to hard chain–hard sphere mixtures in slitlike pores, J. Chem. Phys. **94**, 3183 (1991).
[33] J. Wu, T. Jiang, D.-e. Jiang, Z. Jin, and D. Henderson, A classical density functional theory for interfacial layering of ionic liquids, Soft Matter **7**, 11222 (2011).
[34] Y.-X. Yu and J. Wu, A fundamental-measure theory for inhomogeneous associating fluids, J. Chem. Phys. **116**, 7094 (2002).
[35] Y.-X. Yu and J. Wu, Density functional theory for inhomogeneous mixtures of polymeric fluids, J. Chem. Phys. **117**, 2368 (2002).
[36] L. Fumagalli, A. Esfandiar, R. Fabregas, S. Hu, P. Ares, A. Janardanan, Q. Yang, B. Radha, T. Taniguchi, K. Watanabe, G. Gomila, K. S. Novoselov, and A. K. Geim, Anomalously low dielectric constant of confined water, Science **360**, 1339 (2018).
[37] J.-P. Hansen and I. R. McDonald, *Theory of Simple Liquids: with Applications to Soft Matter* 4th ed. (Academic Press, Amsterdam, 2013).
[38] H. Hansen-Goos and R. Roth, Density functional theory for hard-sphere mixtures: The white bear version mark II, J. Phys. Condens. Matter **18**, 8413 (2006).
[39] L. Blum, Mean spherical model for asymmetric electrolytes, Mol. Phys. **30**, 1529 (1975).
[40] We note that the MSA does not take into account ion clustering, which Härtel *et al.* [17] found to lead to anomalously large screening lengths [17] in simulations of a restricted primitive model in the strong coupling regime.
[41] P. Loche, C. Ayaz, A. Schlaich, D. J. Bonthuis, and R. R. Netz, Breakdown of linear dielectric theory for the interaction between hydrated ions and graphene, J. Phys. Chem. Lett. **9**, 6463 (2018).
[42] E. Gongadze and A. Iglič, Decrease of permittivity of an electrolyte solution near a charged surface due to saturation and excluded volume effects, Bioelectrochem. Bioenerg. **87**, 199 (2012).
[43] F. Fahrenberger, Z. Xu, and C. Holm, Simulation of electric double layers around charged colloids in aqueous solution of variable permittivity, J. Chem. Phys. **141**, 064902 (2014).
[44] F. Fahrenberger, O. A. Hickey, J. Smiatek, and C. Holm, Importance of Varying Permittivity on the Conductivity of Polyelectrolyte Solutions, Phys. Rev. Lett. **115**, 118301 (2015).
[45] A. M. Smith, K. R. J. Lovelock, N. N. Gosvami, T. Welton, and S. Perkin, Quantized friction across ionic liquid thin films, Phys. Chem. Chem. Phys. **15**, 15317 (2013).
[46] R. Buchner, G. T. Hefter, and P. M. May, Dielectric relaxation of aqueous NaCl solutions, J. Phys. Chem. A **103**, 1 (1998).
[47] B. Hess, C. Holm, and N. van der Vegt, Modeling Multi-Body Effects in Ionic Solutions with a Concentration Dependent Dielectric Permittivity, Phys. Rev. Lett. **96**, 147801 (2006).
[48] M. Sega, S. S. Kantorovich, C. Holm, and A. Arnold, Communication: Kinetic and pairing contributions in the dielectric spectra of electrolyte solutions, J. Chem. Phys. **140**, 211101 (2014).
[49] M. Valiskó and D. Boda, The effect of concentration- and temperature-dependent dielectric constant on the activity coefficient of NaCl electrolyte solutions, J. Chem. Phys. **140**, 234508 (2014).
[50] N. Gavish and K. Promislow, Dependence of the dielectric constant of electrolyte solutions on ionic concentration: A microfield approach, Phys. Rev. E **94**, 012611 (2016).
[51] A. A. Lee, C. S. Perez-Martinez, A. M. Smith, and S. Perkin, Underscreening in concentrated electrolytes, Faraday Discuss. **199**, 239 (2017).